Supporting Information

Tailoring the oxygenated groups of graphene hydrogels for high-performance supercapacitors with large areal mass loadings

Hongyun Ma,[a] Qinqin Zhou,[a] Mingmao Wu,[a] Miao Zhang,[a] Bowen Yao,[a] Tiantian Gao,[a] Haiyan Wang,[a] Chun Li,*[a] Dong Sui,[b] Yongsheng Chen,[b] Gaoquan Shi*[a]

[a]Department of Chemistry, MOE Key Laboratory of Bioorganic Phosphorus Chemistry & Chemical Biology, Tsinghua University, Beijing 100084, People's Republic of China.

[b]Key Laboratory of Functional Polymer Materials and Center for Nanoscale Science & Technology, Institute of Polymer Chemistry, College of Chemistry, Nankai University, Tianjin 300071, People's Republic of China.

*Corresponding author: chunli@tsinghua.edu.cn, gshi@tsinghua.edu.cn

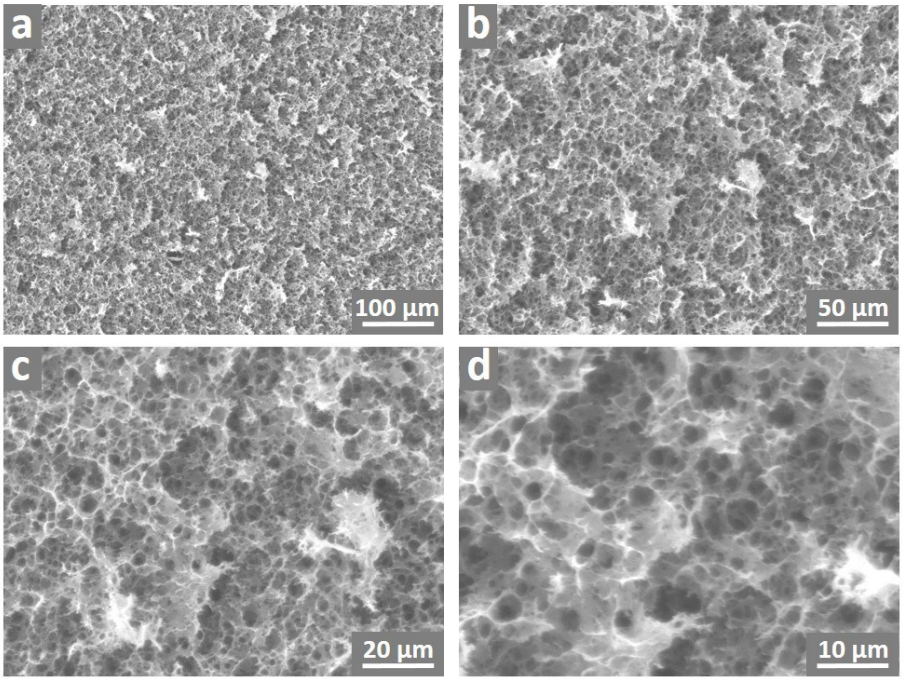

Fig. S1 Typical SEM images of HRGH-0 with different magnifications.

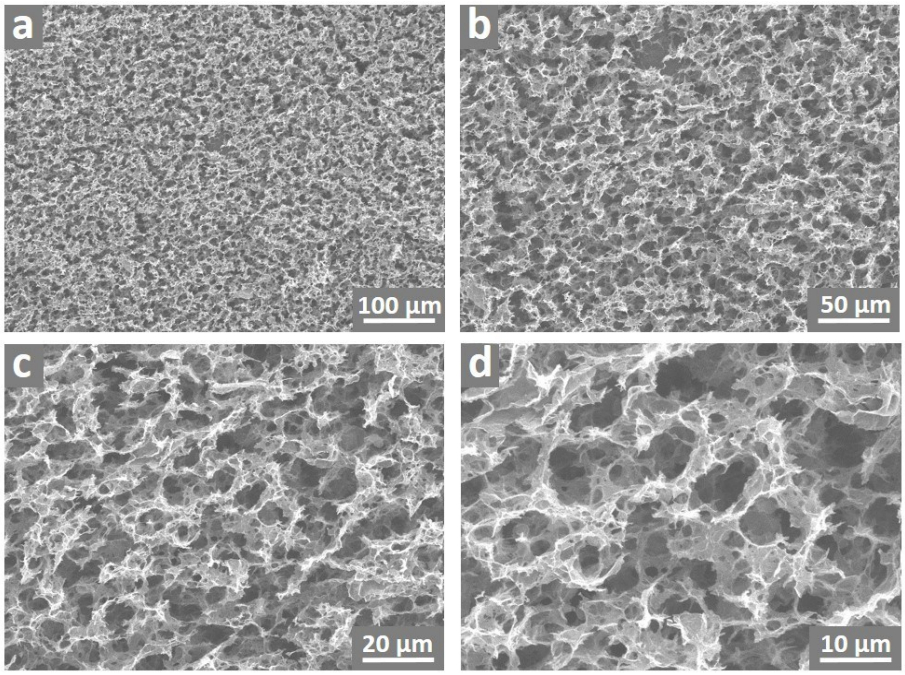

Fig. S2 Typical SEM images of HRGH-0.1 with different magnifications.

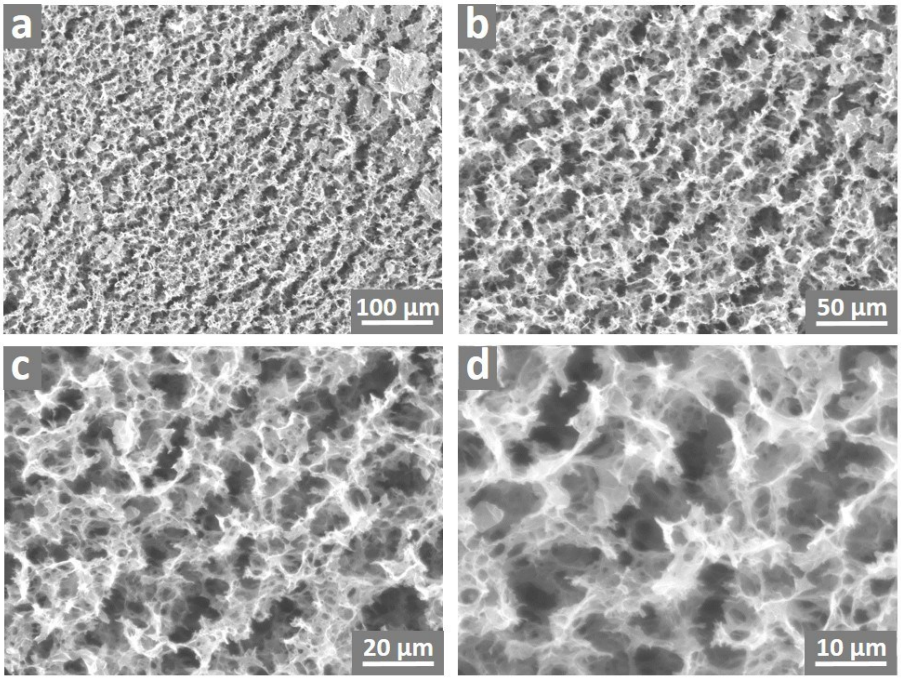

Fig. S3 Typical SEM images of HRGH-0.2 with different magnifications.

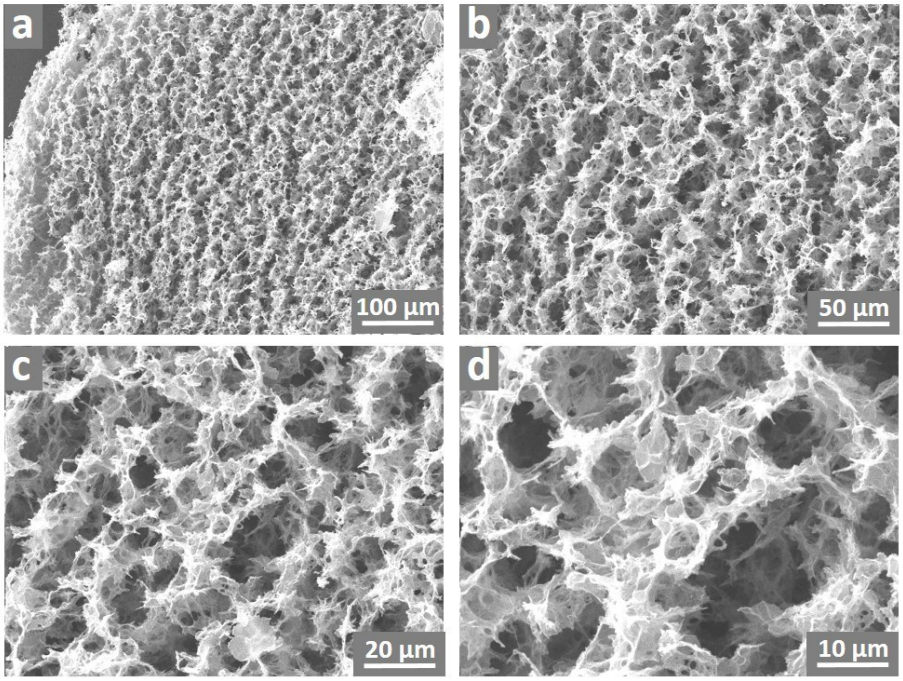

Fig. S4 Typical SEM images of HRGH-0.4 with different magnifications.

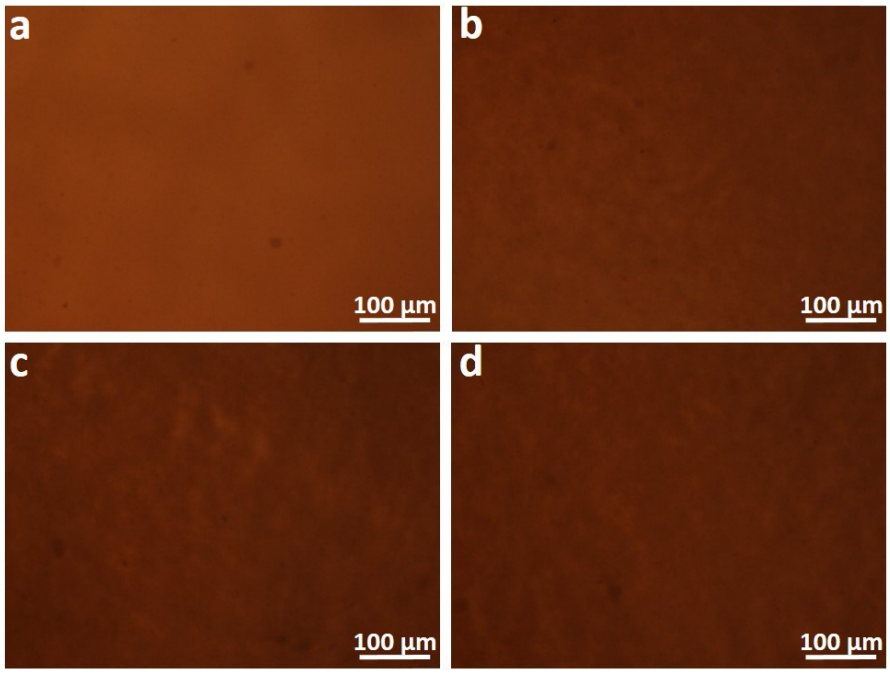

Fig. S5 Optical microscope photographs of GO solutions (2 mg mL^{-1}) containing different concentrations of H_3PO_4: a) 0, b) 0.1, c) 0.2, and d) 0.4 mol L^{-1}.

The optical microscope photographs were taken from GO solutions (2 mg mL^{-1}) containing different concentrations of H_3PO_4. Considering these four photographs were taken by using the same light source with identical intensity, their colors and/or brightness can be used to probe the formation of GO aggregates. Obviously, after adding H_3PO_4 to GO solution, floc-like shadows were gradually appearing, implying the formation of GO aggregates in the H_3PO_4-contianing GO solutions.

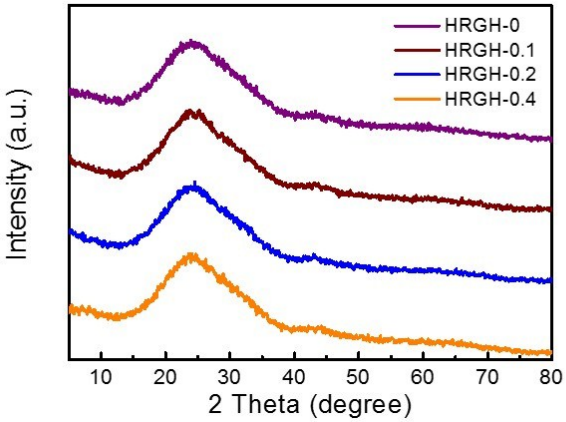

Fig. S6 XRD patterns of HRGH-*n*.

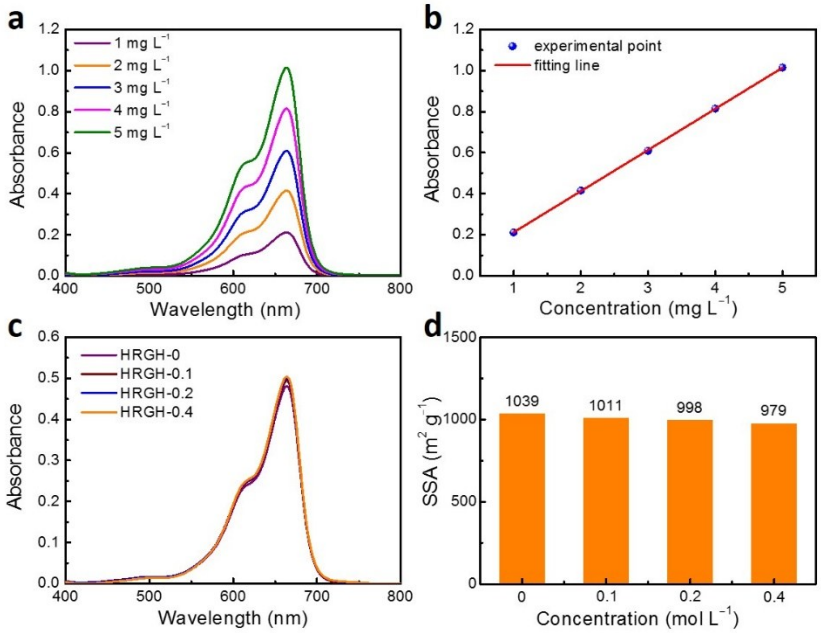

Fig. S7 SSA measurements of HRGH-*n* by a standard methylene blue (MB) adsorption method. a) UV-visible spectra of MB aqueous solutions with different concentrations. b) Standard curve of MB aqueous solutions derived from the peak absorbance at 664 nm. c) UV-visible spectra of MB aqueous solutions after adsorbed by HRGH-*n*. d) SSAs of the HRGH-*n* calculated from MB adsorption method.

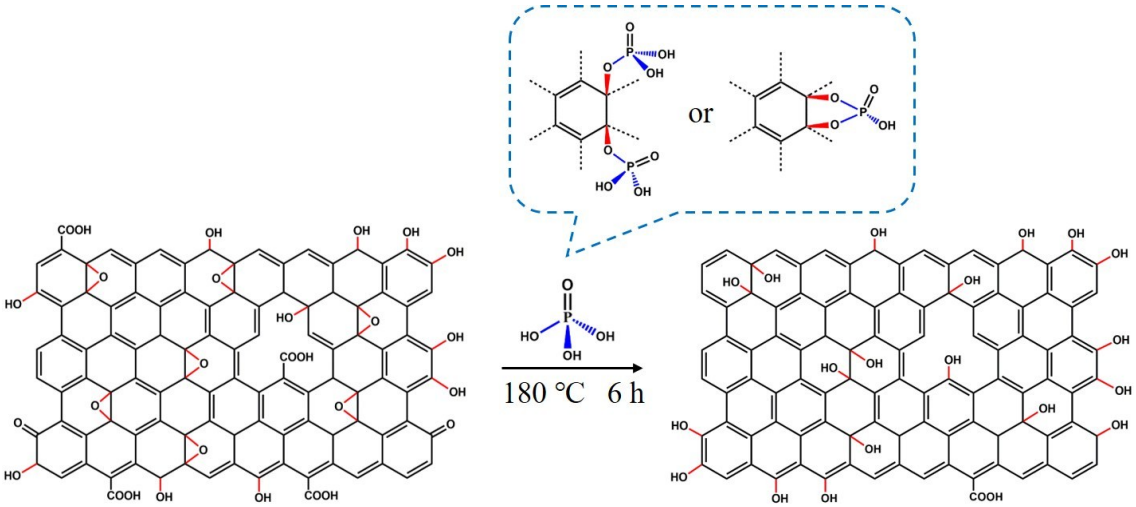

Fig. S8 Schematic illustration of forming HRGH by using phosphorus acid as a protecting agent of hydroxyl groups.

GO sheets have a large amount of oxygenated groups including epoxies, hydroxyls, ketones, and phenols on basal planes, and carboxyls, anhydrates, lactones, phenols, lactols, pyrones and ketones on edges.[S1] According to the observation of Cai *et al.*,[S2] the main oxygenated groups on

GO basal plane are epoxies and hydroxyls, and a hydroxyl group bonded to carbon atom is accompanied by an epoxy group bonded to a neighboring carbon atom. The epoxy groups on GO sheet are easily convered to hydroxyl groups in an acidic medium *via* ring opening reactions; thus, in our case, the main oxygenated groups on GO basal plane can be viewed as hydroxyls. During the H_3PO_4 assisted hydrothermal reduction process, H_3PO_4 reacted with hydroxyl to form phosphate ester and thus restricted the elimination of hydroxyl groups on GO sheets. After hydrothermal reaction, the inverse process, *i.e.* the cleavage of phosphate ester occurred when dialysing the obtained hydrogel in deionized water and the residual H_3PO_4 can be easily removed. As a result, the hydroxyl-rich graphene hydrogel (HRGH) was successfully obtained. As described above, the original hydroxyls and epoxies on GO sheet are bonded to neighboring carbon atoms; thus there are abundant 1,2- or 1,4-phenol structures on the obtained rGO sheets.

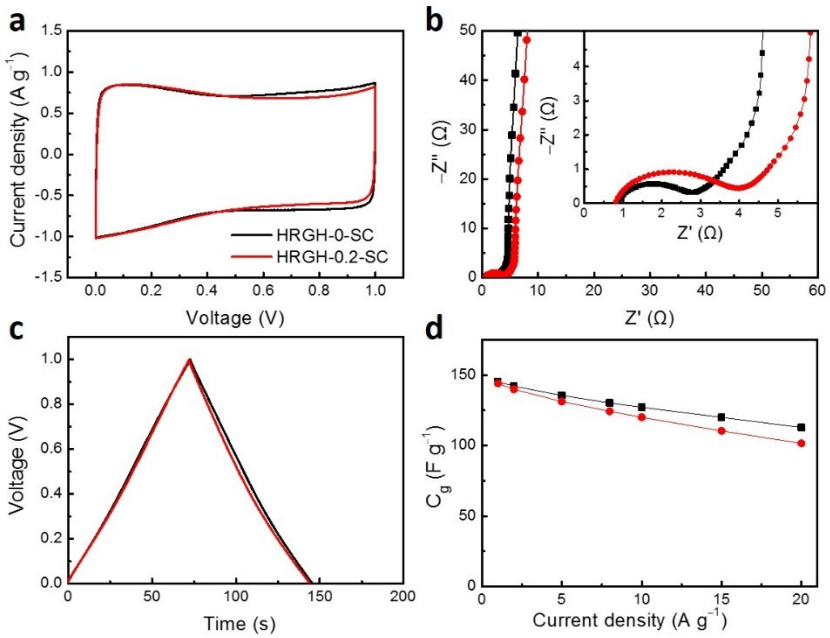

Fig. S9 Electrochemical performances of HRGH-*n*-SCs in neutral electrolyte of 1 mol L^{-1} Na_2SO_4. a) CV curves at a scan rate of 10 mV s^{-1}. b) Nyquist plots. c) GCD curves at a current density of 1 A g^{-1}. d) C_gs at current densities ranging from 1 to 20 A g^{-1}.

The phenol hydroxyls in ortho- or para-positions of 6-memberd carbon rings can electrochemically convert to 1,2- or 1,4-quinones upon oxidation, and thus contribute pseudo-capacitance (Fig. S13). It should be noted that these pseudo-capacitive reactions only take place in acidic system (e.g. H_2SO_4). Therefore, the specific capacitances of HRGH-*n*-SCs tested in nutral system (e.g. Na_2SO_4) can be assigned only to electric double layer (EDL) capacitances.

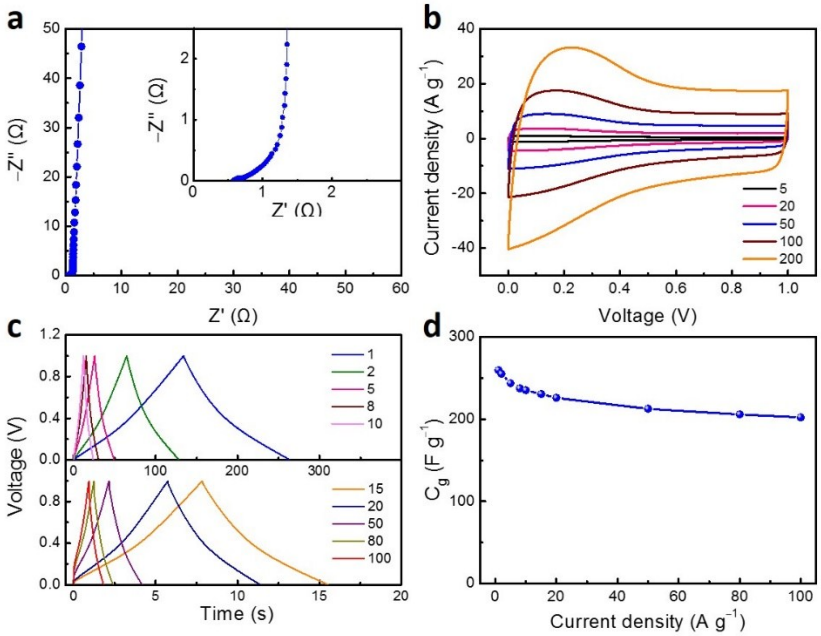

Fig. S10 Electrochemical performances of HRGH-0.2-SC. a) Nyquist plot. b) CV curves at scan rates ranging from 5 to 200 mV s^{-1}. c) GCD curves at current densities ranging from 1 to 100 A g^{-1}. d) C_gs at current densities ranging from 1 to 100 A g^{-1}.

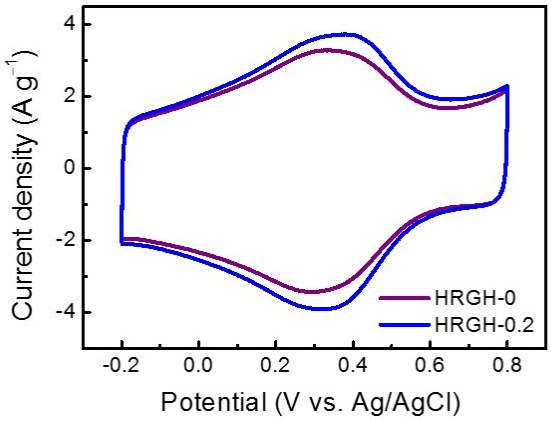

Fig. S11 CV curves (10 mV s^{-1}) of HRGH-*n* tested in a three-electrode configuration by using 1 mol L^{-1} H_2SO_4 as the electrolyte, a Pt plate as the counter electrode, and Ag/AgCl as the reference electrode.

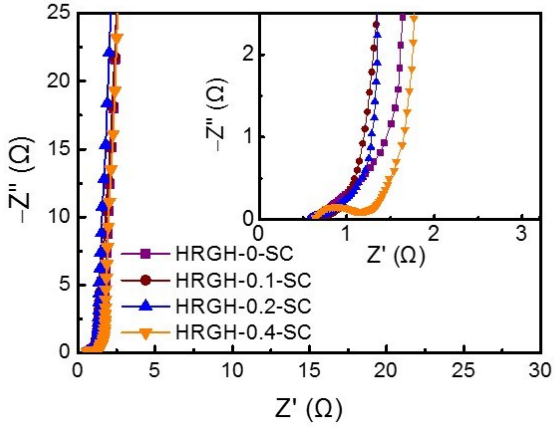

Fig. S12 Nyquist plots of HRGH-*n*-SCs.

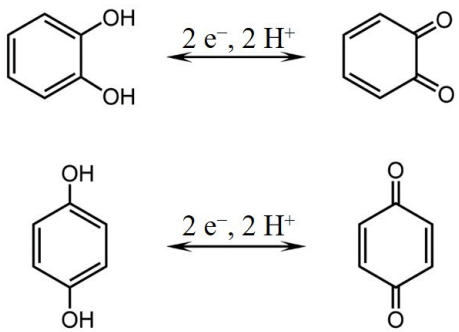

Fig. S13 Reaction mechanism of the reversible electrochemical conversions between 1,2- or 1,4-phenol structures and 1,2- or 1,4-quinone structures on rGO sheets.

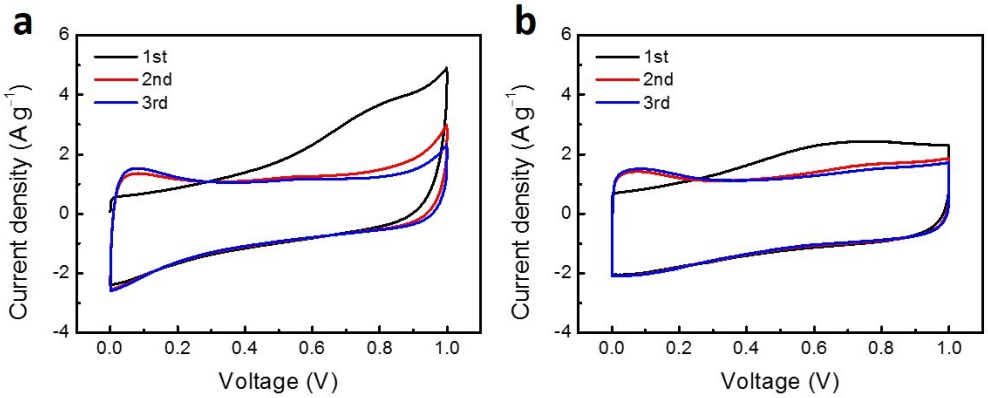

Fig. S14 First three CV curves of a) NTGH-based supercapacitor or b) HRGH-0.2-SC at a scan rate of 10 mV s^{-1}.

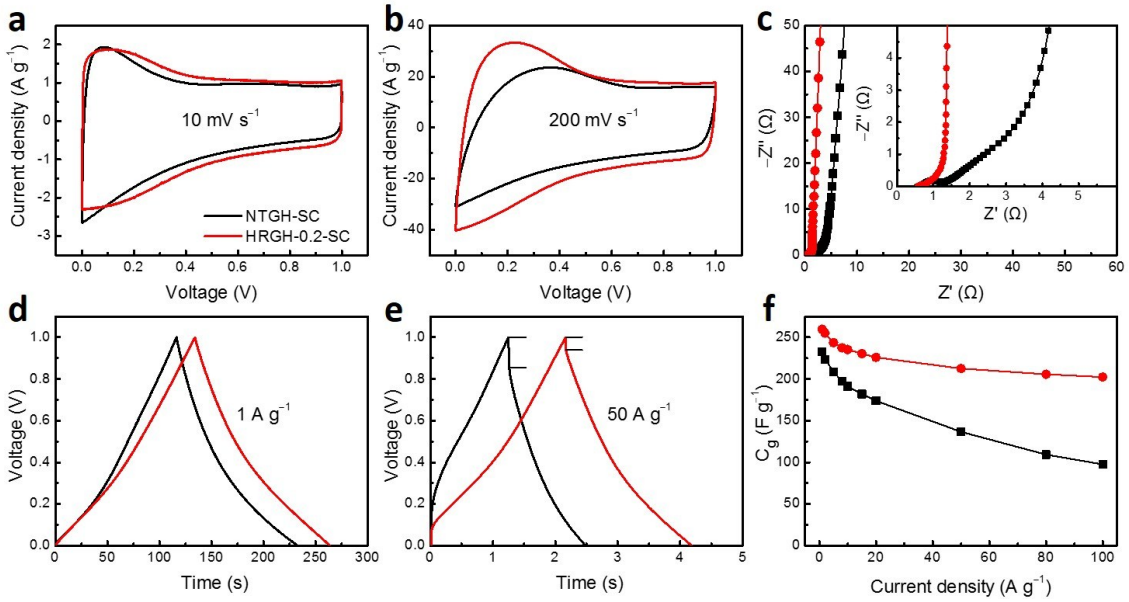

Fig. S15 Electrochemical performances of NTGH based supercapacitor in comparision with those of HRGH-0.2-SC. a) CV curves at a scan rate of 10 mV s^{-1}. b) CV curves at a scan rate of 200 mV s^{-1}. c) Nyquist plots. d) GCD curves at a current density of 1 A g^{-1}. e) GCD curves at a current density of 50 A g^{-1}. f) C_gs at current densities ranging from 1 to 100 A g^{-1}.

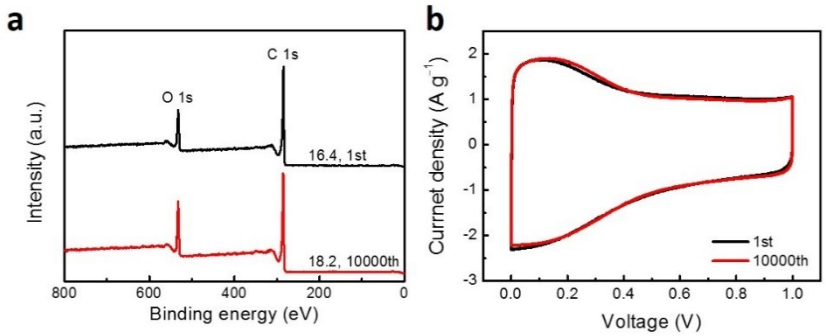

Fig. S16 XPS surveys a) and CV curves b) of HRGH-0.2 before and after 10,000 charge/discharge cycles.

As shown in Fig. S16a, the intensity of O 1s for HRGH-0.2 was getting larger after 10,000 charge/discharge cycles. This might be caused by the different state of surface oxidation (open circuit potential) before and after cycling stability test. Nevertheless, the CV curve after 10,000 charge/discharge cycles almost coincided with the original one, reflecting the excellent cycling stability of HRGH-0.2-SC (Fig. S16b).

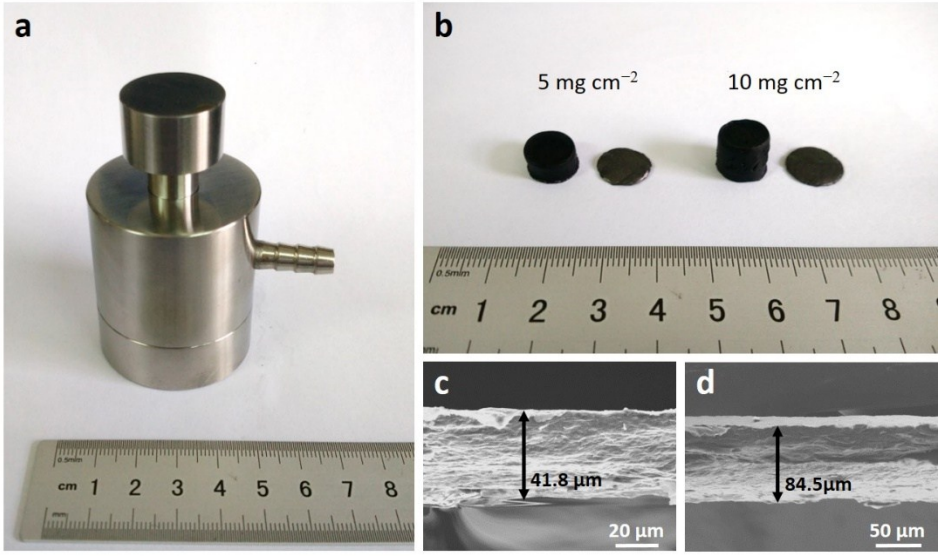

Fig. S17 Preparation of compact HRGH-0.2 electrodes with high areal mass loadings. a) Digital image of the stainless steel mould. b) Digital images of HRGH-0.2 electrodes before and after mechanical compression. c, d) SEM images of the cross section of compressed HRGH-0.2 electrodes: c) 5 mg cm^{-2}, and d) 10 mg cm^{-2}.

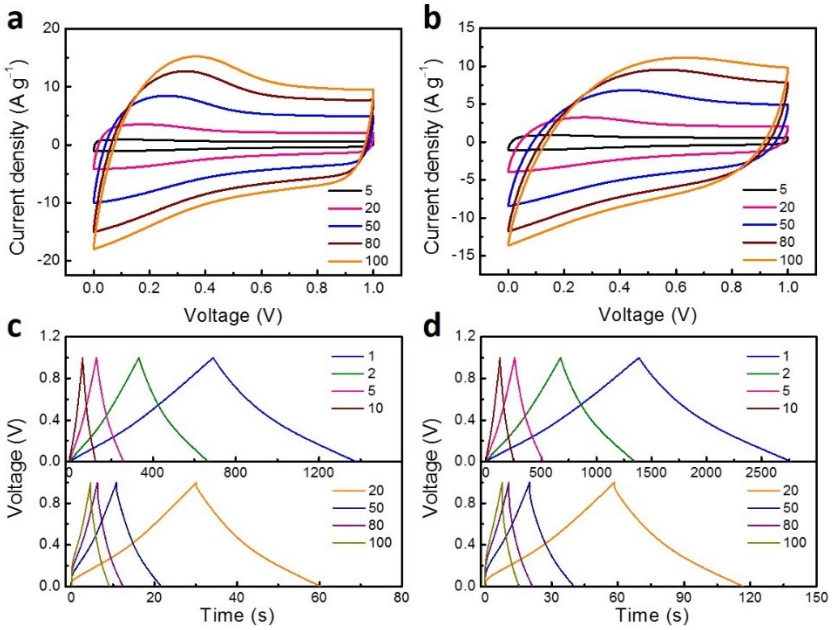

Fig. S18 CV curves of the HRGH-0.2-SC with a) 5 or b) 10 mg cm^{-2} mass loading at scan rates ranging from 5 to 100 mV s^{-1}. GCD curves of the HRGH-0.2-SC with c) 5 or d) 10 mg cm^{-2} mass loading at current densities ranging from 1 to 100 mA cm^{-2}.

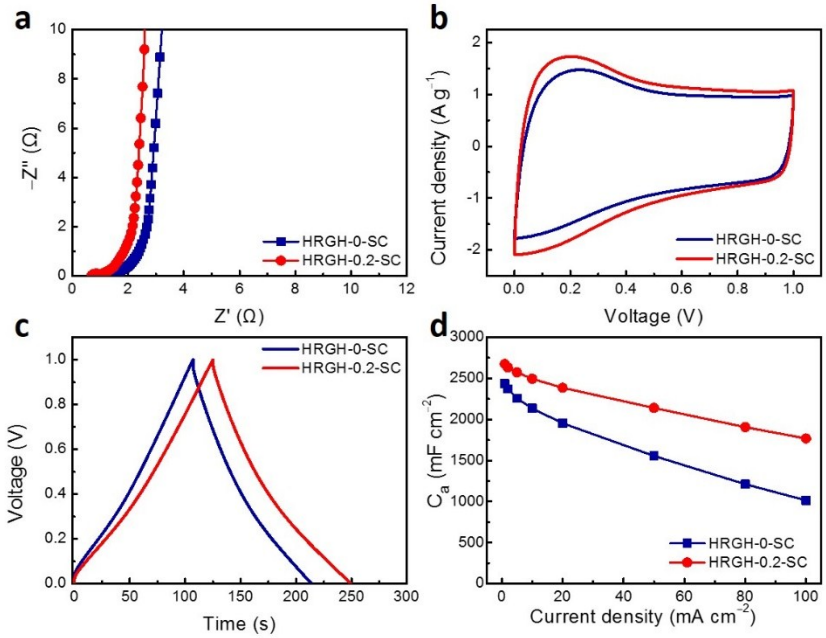

Fig. S19. Electrochemical performances of HRGH-*n*-SCs with a high areal mass loading of 10 mg cm^{-2}. a) Nyquist plots. b) CV curves at a scan rate of 10 mV s^{-1}. c) GCD curves at a current density of 10 mA cm^{-2}. d) C_as at current densities ranging from 1 to 100 mA cm^{-2}.

Table S1. The SSAs, I_D/I_Gs, L_Ds, oxygen atomic contents, and conductivities of HRGH-*n*.

	SSA (m^2 g^{-1})	I_D/I_G	L_D	Oxygen atomic content (at.%)	Conductivity (S m^{-1})
HRGH-0	1039	1.11	1.52	15.5	106
HRGH-0.1	1011	1.09	1.50	15.8	97
HRGH-0.2	998	1.07	1.48	16.4	92
HRGH-0.4	979	1.04	1.45	16.8	76

Table S2. Dynamic water contact angles of HRGH-*n*.

	0 s	20 s	40 s	60 s	80 s	100 s	120s
HRGH-0	79.5°	72.3°	62.6°	46.9°	31.9°	19.3°	0
HRGH-0.1	68.4°	60.5°	48.3°	33.5°	17.6°	0	0
HRGH-0.2	45.8°	32.2°	15.5°	0	0	0	0
HRGH-0.4	31.3°	16.6°	0	0	0	0	0

Table S3. Comparison of the C_vs of reported carbon- or graphene-based materials.

Material	Electrolyte	System	Rate	C_g (F g^{-1})	C_v (F cm^{-3})	Ref.
HRGH-0.2	**1 M H_2SO_4**	***A***	**1 A g^{-1}**	**260**	**312**	**This work**
Carbon sphere	30% KOH	*A*	2 mV s^{-1}	164	170	S3
Activated carbon	6 M KOH	*A*	1 mV s^{-1}	339	171	S4
N-doped carbon fiber	6 M KOH	*B*	1 A g^{-1}	202	200	S5
N-doped porous carbon	1 M H_2SO_4	*B*	0.2 A g^{-1}	298	161	S6
B-/N-porous carbon	6 M KOH	*B*	0.5 A g^{-1}	247	101	S7
N,P co-doped carbon	1 M H_2SO_4	*B*	0.5 A g^{-1}	206	261	S8
CNFs [a]	6 M KOH	*B*	0.5 A g^{-1}	280	88	S9
3D porous carbon	6 M KOH	*B*	0.5 A g^{-1}	318	118	S10
Porous carbon films	0.5 M H_2SO_4	*B*	10 mV s^{-1}	180	220	S11
MCMB [b]	6 M KOH	*A*	0.2 A g^{-1}	306	160	S12
Carbon aerogel	1 M H_2SO_4	*B*	0.2 A g^{-1}	251	166	S13
ACM [c]	6 M KOH	*A*	0.05 A g^{-1}	348	162	S14
Porous carbon	6 M KOH	*B*	2 mV s^{-1}	271	252	S15
Porous carbon	1 M H_2SO_4	*A*	2 mV s^{-1}	198	180	S16
Porous carbon	6 M KOH	*A*	0.05 A g^{-1}	262	214	S17
CDC [d]	1 M H_2SO_4	*A*	2 mV s^{-1}	190	140	S18
MWNTs [e]	1 M H_2SO_4	*B*	50 mV s^{-1}	159	132	S19
EM-CCG [f]	1 M H_2SO_4	*A*	0.1 A g^{-1}	203	256	S20
NS-rGO [g]	6 M KOH	*A*	1 A g^{-1}	237	51.4	S21
Graphene film	6 M KOH	*A*	0.1 A g^{-1}	226	174	S22
VArGO [h]	6 M KOH	*A*	0.05 A g^{-1}	145	171	S23
3D HPG [i]	6 M KOH	*A*	0.5 A g^{-1}	305	177	S24
3D graphene	1 M H_2SO_4	*A*	1 A g^{-1}	250	30	S25
RGO-HD [j]	6 M KOH	*A*	1 A g^{-1}	182	255	S26
HPGM [k]	6 M KOH	*A*	0.1 A g^{-1}	238	376	S27
Holey graphene	6 M KOH	*A*	1 A g^{-1}	310	221	S28
S-carbon/graphene	6 M KOH	*A*	0.05 A g^{-1}	109	65	S29

A or *B* refers to two- or three-electrode system.

[a] CNFs: mesoporous carbon nanofibers; [b] MCMB: coal-tar pitch derived mesocarbon microbeads; [c] ACM: amphiphilic carbonaceous material; [d] CDC: carbide derived carbons; [e] MWNTs: multiwall carbon nanotube thin films; [f] EM-CCG: electrolyte-mediated chemically converted graphene films; [g] NS-rGO: non-stacked reduced graphene oxide powders; [h] VArGO: vertically-aligned reduced graphene oxide electrodes; [i] 3D HPG: three-dimensional hierarchical porous graphene-like networks; [j] RGO-HD: high density reduced graphite oxide; [k] HPGM: high density porous graphene macroform.

Table S4. Areal capacitance comparison of the carbon- or graphene-based symmetric supercapacitors with high areal mass loadings.

Material	Mass loading (mg cm^{-2})	Rate	C_a (mF cm^{-2})	Ref.
HRGH-0.2	**10**	**1 mA cm^{-2}**	**2675**	**This work**
		50 mA cm^{-2}	**2140**	
		100 mA cm^{-2}	**1768**	
PANI/CNT/paper [a]	3.32	10 mA cm^{-2}	1506	S30
		100 mA cm^{-2}	1298	
Holey Graphene Discs	30	7.5 mA cm^{-2}	1300	S31
		30 mA cm^{-2}	860	
N-CNFs/RGO/BC [b]	16	2 mA cm^{-2}	920	S32
		50 mA cm^{-2}	755	
3D SMG [c]	6.4	3.2 mA cm^{-2}	1280	S33
		32 mA cm^{-2}	~1000	
CNC-MWCNT-PPy [d]	17.8	2 mV s^{-1}	2100	S34
		100 mV s^{-1}	<300	
3D CFG [e]	11.16	1 A g^{-1}	1160	S35
		10 A g^{-1}	~900	
CNFs [f]	60	1 mA cm^{-2}	1200	S36
		60 mA cm^{-2}	~900	
PPy@c-NCFs [g]	9	1 mA cm^{-2}	<1620	S37
		300 mA cm^{-2}	1122	
AWC [h]	30	1 mA cm^{-2}	3600	S38
		20 mA cm^{-2}	1300	

[a] PANI/CNT/paper: the stacking up layers of polyaniline/carbon nanotube composite networks inside air-laid papers; [b] N-CNFs/RGO/BC: nitrogen-doped carbon nanofiber networks/reduced graphene oxide/bacterial cellulose freestanding paper; [c] 3D SMG: three-dimensional surface-microporous graphene; [d] CNC-MWCNT-PPy: the *in situ* polymerized polypyrrole in an aerogel-based current collector composed of cross-linked cellulose nanocrystals and multi-walled carbon nanotubes; [e] 3D CFG: three-dimensional cauliflower-fungus-like graphene material; [f] CNFs: carbon nanofibers; [g] PPy@c-NCFs: polypyrrole@cationic nanocellulose fibers; [h] AWC: activated wood carbon.

Supplementary References

S1 A. Bagri, C. Mattevi, M. Acik, Y. J. Chabal, M. Chhowalla and V. B. Shenoy, *Nat. Chem.*, 2010, **2**, 581–587.

S2 W. Cai, R. D. Piner, F. J. Stadermann, S. Park, M. A. Shaibat, Y. Ishii, D. Yang, A. Velamakanni, S. J. An, M. Stoller, J. An, D. Chen and R. S. Ruoff, *Science*, 2008, **321**, 1815–1817.

S3 X. H. Xia, L. Shi, H. B. Liu, L. Yang and Y. D. He, *J. Phys. Chem. Solids*, 2012, **73**, 385–390.

S4 B. Xu, Y. F. Chen, G. Wei, G. P. Cao, H. Zhang and Y. S. Yang, *Mater. Chem. Phys.*, 2010, **124**, 504–509.

S5 L.-F. Chen, X.-D. Zhang, H.-W. Liang, M. Kong, Q.-F. Guan, P. Chen, Z.-Y. Wu and S.-H. Yu, *ACS Nano*, 2012, **6**, 7092–7102.

S6 L. Hao, B. Luo, X. L. Li, M. H. Jin, Y. Fang, Z. H. Tang, Y. Y. Jia, M. H. Liang, A. Thomas, J. H. Yang and L. J. Zhi, *Energy Environ. Sci.*, 2012, **5**, 9747–9751.

S7 D. C. Guo, J. Mi, G. P. Hao, W. Dong, G. Xiong, W. C. Li and A. H. Lu, *Energy Environ. Sci.*, 2013, **6**, 652–659.

S8 X. Yan, Y. Yu, S.-K. Ryu, J. Lan, X. Jia and X. Yang, *Electrochim. Acta*, 2014, **136**, 466–472.

S9 W. Li, F. Zhang, Y. Q. Dou, Z. X. Wu, H. J. Liu, X. F. Qian, D. Gu, Y. Y. Xia, B. Tu and D. Y. Zhao, *Adv. Energy Mater.*, 2011, **1**, 382–386.

S10 L. Qie, W. Chen, H. Xu, X.-Q. Xiong, Y. Jiang, F. Zou, X. Hu, Y. Xin, Z. Zhang and Y. Huang, *Energy Environ. Sci.*, 2013, **6**, 2497–2504.

S11 Z. Lausevic, P. Y. Apel, J. B. Krstic and I. V. Blonskaya, *Carbon*, 2013, **64**, 456–463.

S12 K. Torchala, K. Kierzek and J. Machnikowski, *Electrochim. Acta*, 2012, **86**, 260–267.

S13 Z. Zapata-Benabithe, F. Carrasco-Marin, J. de Vicente and C. Moreno-Castilla, *Langmuir*, 2013, **29**, 6166–6173.

S14 J. Wang, M. M. Chen, C. Y. Wang, J. Z. Wang and J. M. Zheng, *J. Power Sources*, 2011, **196**, 550–558.

S15 J. A. Hu, H. L. Wang, Q. M. Gao and H. L. Guo, *Carbon*, 2010, **48**, 3599–3606.

S16 E. Raymundo-Pinero, F. Leroux and F. Beguin, *Adv. Mater.*, 2006, **18**, 1877–1882.

S17 B. Xu, F. Wu, S. Chen, Z. M. Zhou, G. P. Cao and Y. S. Yang, *Electrochim. Acta*, 2009, **54**, 2185–2189.

S18 J. Chmiola, G. Yushin, R. Dash and Y. Gogotsi, *J. Power Sources*, 2006, **158**, 765–772.

S19 S. W. Lee, B. S. Kim, S. Chen, Y. Shao-Horn and P. T. Hammond, *J. Am. Chem. Soc.*, 2009, **131**, 671–679.

S20 X. Yang, C. Cheng, Y. Wang, L. Qiu and D. Li, *Science*, 2013, **341**, 534–537.

S21 Y. Yoon, K. Lee, C. Baik, H. Yoo, M. Min, Y. Park, S. M. Lee and H. Lee, *Adv. Mater.*, 2013, **25**, 4437–4444.

S22 Z. Lei, L. Lu and X. S. Zhao, *Energy Environ. Sci.*, 2012, **5**, 6391–6399.

S23 Y. Yoon, K. Lee, S. Kwon, S. Seo, H. Yoo, S. Kim, Y. Shin, Y. Park, D. Kim, J.-Y. Choi and H. Lee, *ACS Nano*, 2014, **8**, 4580–4590.

S24 Y. Li, Z. Li and P. K. Shen, *Adv. Mater.*, 2013, **25**, 2474–2480.

S25 X. Wang, Y. Zhang, C. Zhi, X. Wang, D. Tang, Y. Xu, Q. Weng, X. Jiang, M. Mitome, D. Golberg and Y. Bando, *Nat. Commun.*, 2013, **4**, 2905.

S26 Y. Li and D. Zhao, *Chem. Commun.*, 2015, **51**, 5598–5601.

S27 Y. Tao, X. Xie, W. Lv, D.-M. Tang, D. Kong, Z. Huang, H. Nishihara, T. Ishii, B. Li, D. Golberg, F. Kang, T. Kyotani and Q.-H. Yang, *Sci. Rep.*, 2013, **3**, 2975.

S28 Y. X. Xu, Z. Y. Lin, X. Zhong, X. Q. Huang, N. O. Weiss, Y. Huang and X. F. Duan, *Nat. Commun.*, 2014, **5**, 4554.

S29 M. Seredych and T. J. Bandosz, *J. Mater. Chem. A*, 2013, **1**, 11717–11727.

S30 L. Dong, G. Liang, C. Xu, D. Ren, J. Wang, Z.-Z. Pan, B. Li, F. Kang and Q.-H. Yang, *J. Mater. Chem. A*, 2017, **5**, 19934–19942.

S31 E. D. Walsh, X. Han, S. D. Lacey, J.-W. Kim, J. W. Connell, L. Hu and Y. Lin, *ACS Appl. Mater. Interfaces*, 2016, **8**, 29478–29485.

S32 L. Ma, R. Liu, H. Niu, L. Xing, L. Liu and Y. Huang, *ACS Appl. Mater. Interfaces*, 2016, **8**, 33608–33618.

S33 L. Chang, D. J. Stacchiola and Y. H. Hu, *ACS Appl. Mater. Interfaces*, 2017, **9**, 24655–24661.

S34 K. Shi, X. Yang, E. D. Cranston and I. Zhitomirsky, *Adv. Funct. Mater.*, 2016, **26**, 6437–6445.

S35 L. Chang, W. Wei, K. Sun and Y. H. Hu, *J. Mater. Chem. A*, 2015, **3**, 10183–10187.

S36 J. R. McDonough, J. W. Choi, Y. Yang, F. La Mantia, Y. Zhang and Y. Cui, *Appl. Phys. Lett.*, 2009, **95**, 243109.

S37 Z. Wang, D. O. Carlsson, P. Tammela, K. Hua, P. Zhang, L. Nyholm and M. Stromme, *ACS Nano*, 2015, **9**, 7563–7571.

S38 C. Chen, Y. Zhang, Y. Li, J. Dai, J. Song, Y. Yao, Y. Gong, I. Kierzewski, J. Xie and L. Hu,

Energy Environ. Sci., 2017, **10**, 538–545.